Available online at www.sciencedirect.com
ScienceDirect
Ceramics International 34 (2008) 1579–1586
CERAMICS INTERNATIONAL
www.elsevier.com/locate/ceramint

Influence of porosity on the electrical properties of $La_{9.33}(SiO_4)_6O_2$ oxyapatite

P.J. Panteix [a,b,*], I. Julien [b], P. Abélard [b], D. Bernache-Assollant [c]

[a] Centre Interuniversitaire de Recherche et d'Ingénierie des Matériaux, UMR 5085, Université Paul Sabatier, 118 Route de Narbonne, 31062 Toulouse Cedex 4, France
[b] Science des Procédés Céramiques et de Traitements de Surface, Université de Limoges, UMR 6638, 123 Avenue Albert Thomas, 87060 Limoges Cedex, France
[c] Ecole Nationale Supérieure des Mines, 158 Cours Fauriel, 42023 Saint-Etienne Cedex 2, France

Received 8 March 2007; received in revised form 10 April 2007; accepted 2 May 2007
Available online 2 June 2007

Abstract

Oxyapatites are very promising materials in terms of ionic conductivity. They can be considered as a potential electrolyte for fuel cells as SOFC. The influence of porosity on the electrical properties of $La_{9.33}(SiO_4)_6O_2$ oxyapatite is reported here. Hot pressed pellets with various densification ratios have been characterized by the complex impedance method. The high frequency response associated with the bulk contribution is much more affected by the porosity than the grain boundaries contribution: as a consequence, the electrical behaviour of the samples has been considered in assimilating the porous ceramics to composite materials made of apatite with various amounts of air inclusions. Thus, the porosity dependence of conductivity, activation energy and permittivity are reported here. A percolation threshold has been highlighted for porosity values greater than 30%, involving great lowering of the electrical performances.

Keywords: A. Hot pressing; B. Porosity; C. Electrical properties; D. Apatite

1. Introduction

The use of SOFC at intermediate temperatures (from 600 to 800 °C) is mainly limited by the electrolyte properties. One of the most used electrolytes is yttria-stabilized zirconia YSZ [1–4], which is well-known as an excellent oxygen conducting electrolyte at temperatures beyond 1000 °C. Apatites seem to be very promising to be used as oxide ions conductors at intermediate temperatures (700–800 °C). Indeed, the presence of large conduction channels containing oxide ions O^{2-} may suggest that materials with the apatite structure should be appropriated for such an application. A wide variety of materials crystallize in the hexagonal apatite structure (mineral formula $Me_{10}(XO_4)_6Y_2$, space group $P6_3/m$). Me represents a divalent cation, XO_4 a trivalent anion and Y a monovalent anion. Me^{2+} cations are located in two different sites: $4Me_I$ are at the centre of narrow tunnels (4f), $6Me_{II}$ around large tunnels (6h) the centers of which are occupied by Y^- anions located on the hexad axis (2a). The coordination number of Me_I site is nine, whereas for Me_{II}, it is only seven [5]. A lot of substitutions can be observed in the apatite structure. As a consequence, many apatites are well-known as one-dimensional anionic conductors. Rare earth silicated oxyapatites as $La_{9.33}\square_{0.67}(SiO_4)_6O_2$ seem to be very attractive in terms of oxide ions conductivity: oxide ions are located on the hexad axis at the centre of the large tunnels, which through they can circulate [6–9].

Many authors have already reported the good electrical performances of oxyapatites: the stoichiometry of these materials is pretty easy to control, and their conductivity can be significantly improved this way: many previous works have reported detailed studies about the electrical properties of substituted oxyapatites [10–22]. This paper deals with the study of the influence of porosity on the electrical properties of $La_{9.33}(SiO_4)_6O_2$. Rare earth silicate oxyapatites are generally prepared by solid-state synthesis. The low specific areas of

* Corresponding author at: Centre Interuniversitaire de Recherche et d'Ingénierie des Matériaux, UMR 5085, Université Paul Sabatier, 118 Route de Narbonne, 31062 Toulouse cedex 4, France. Tel.: +33 5 61 55 61 20; fax: +33 5 61 55 61 63.
E-mail address: panteix@chimie.ups-tlse.fr (P.J. Panteix).

0272-8842/$34.00
doi:10.1016/j.ceramint.2007.05.004

those powders lead to limited densification ratios, even when the sintering is performed at high temperatures (>1400 °C). We have previously reported that the porosity tends to lower the global electrical performances of this material [23]: as a consequence, it might be interesting to determine how much electrical properties are affected by the porosity. Other studies report such results for other ionic conductors as YSZ [24–31] BIMEVOX [32,33], ceria [34,35], LAMOX [36]. The same kind of work is proposed here for oxyapatite. $La_{9.33}(SiO_4)_6O_2$ powder has been prepared by solid state reaction synthesis. Densification of the powder by hot pressing gave several pellets with very close microstructural topology (average grain size, grain size repartition) and various densification ratios. The porosity dependence of some electrical properties (activation energy, conductivity, dielectric permittivity) has been observed in taking this assumption into account. Some theoretical laws relevant to composite materials were also considered in order to explain the electrical behavior of sintered oxyapatite.

2. Materials and methods

2.1. Powder synthesis

Powders of La_2O_3 (Aldrich, 99.9%), SiO_2 (Prolabo, 99%), were used as starting materials. Weight loss of hygroscopic lanthanum oxide was determined by thermogravimetry before weighing, using the TA INSTRUMENTS SDT 2960. Appropriate amounts were mixed in ethanol and ground in a ball-mill (30 min, 180 rpm). The dried powder was then heated up to 1450 °C for 3 h, twice. An intermediate grinding was included between the two thermal treatments in order to improve the reactivity and the homogeneity of the powder. Attrition has been performed for 1 h in ethanol at 490 rpm using a UNION PROCESS 01-Lab Attritor.

2.2. Densification

Hot pressing has been performed using graphite mould and piston under argon. A displacement sensor giving a parallel dilatometric analysis was placed on the piston. The pressure was applied at the beginning of the heating process. The heating rate was 40 °C/min.

2.3. Characterizations

Powder X-ray diffraction (XRD) patterns were recorded with Cu Kα radiation in the 2θ range 17–120° on a $\theta/2\theta$ diffractometer (Siemens, Model D5000, Germany) (θ = diffraction angle). The crystalline phases were identified from a comparison of the registered patterns with the international center for diffraction data (ICDD) powder diffraction files (PDF).

The specific areas of the powders were measured by Brunauer, Emmet and Teller (BET) method (8 points, analyzer Micromeritics ASAP 2010, USA), after degassing under vacuum at 200 °C. Particle size of the powders was determined using a CILAS 1064 analyzer.

The relative densities of the sintered samples were obtained by Archimedes' method in water. Calculations were performed by using the $La_{9.33}(SiO_4)_6O_2$ theoretical density which is equal to 5.319. This result has been confirmed by helium pycnometry measurement (analyze Micromeritics ACCUPIC 1330, USA).

Scanning electron microscopy (SEM) was used for microstructural investigations (Hitachi S2500, Japan). Microstructure of the densified samples was revealed after polishing with SiC paper by a thermal treatment 50 °C below the sintering temperature. The grain size repartitions were determined using the software OptiLab™/Pro-F2.1.6.

Electrical properties have been measured using a SOLARTRON 1260 Impedance/Gain Phase Analyzer. Measurements have been performed after both sides of the sintered disc were coated with Ag paste. The measurements have been made in the frequency range 1 Hz–5 MHz at different temperatures rising from 400 to 800 °C. Impedance plots have been fitted with the software Zlive [37].

3. Results and discussion

3.1. Powder synthesis

Results about the solid-state reaction synthesis have already been reported elsewhere [23]. X-ray diffraction pattern shows that the powder presents relatively high purity with a little amount of the lanthanum silicate $La_2Si_2O_7$ as a secondary phase. This impurity has a La/Si ratio that differs from the desired apatite, so it is supposed that the stoichiometry of the synthesized apatite phase lightly differs from $La_{9.33}(SiO_4)_6O_2$.

Attrition grinding homogenized the particle size of the powder (Fig. 1): the mean grain size is about 1.5 μm. No grain larger than 7 μm is detected. SEM micrograph (Fig. 2) confirms that the powder is not agglomerated. Attrition grinding raised the specific area from 0.51 ± 0.01 to 2.21 ± 0.03 $m^2\ g^{-1}$.

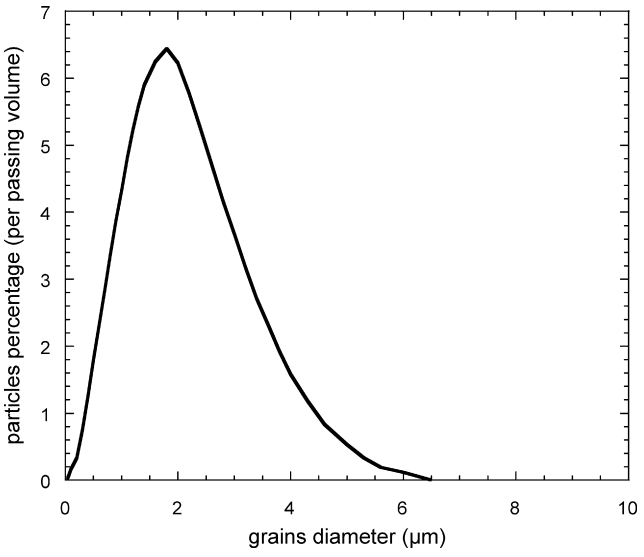

Fig. 1. Grain size repartition of synthesized $La_{9.33}(SiO_4)_6O_2$ powder.

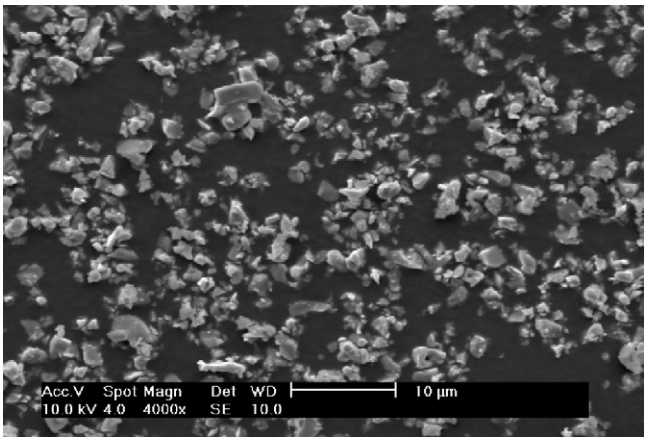

Fig. 2. Scanning electron micrograph of synthesized $La_{9.33}(SiO_4)_6O_2$ powder.

3.2. Powder densification

Samples have been hot pressed at various temperatures (from 1350 to 1400 °C) and under various pressures (24–35 MPa) in order to obtain several densification ratios, varying from 67 to 93% of the theoretical value.

The scanning electron micrographs of the polished surface of four pellets (with porosities equal to 12, 22, 30 and 30%) are presented in Fig. 3. Microstructural characterization has been achieved after image analyses: all average grain sizes were 1.0 ± 0.1 μm, with standard deviations of 0.6 ± 0.1 μm. As a consequence, all hot pressed samples have very close microstructures with different densification ratios. Furthermore, porosity seems to be exclusively intergranular.

3.3. Electrical properties

The influence of porosity on the electrical properties of hot pressed oxyapatite has been studied on seven samples with porosity equal to 7, 12, 14, 19, 22, 30 and 33%.

3.3.1. Raw results

Impedance plots refinements were made at 500 °C in order to make accurate comparisons between electrical properties of all the pellets: indeed, the best refinements were obtained at this temperature. The electrode–electrolyte contribution in the low frequency region is too uncertain to accurately refine the plots at lower temperatures, and the high frequency circle is not wholly recorded for the highest temperatures.

Fig. 4(a) and (b) shows impedance plots at 500 °C in a Nyquist format of all the analyzed pellets. The complex modulus have been determined as follow:

$$M^* = Z^* j\omega\varepsilon_0$$

where M^*, Z^*, ω, ε_0 are the complex modulus, the complex impedance, the angular frequency and the vacuum permittivity

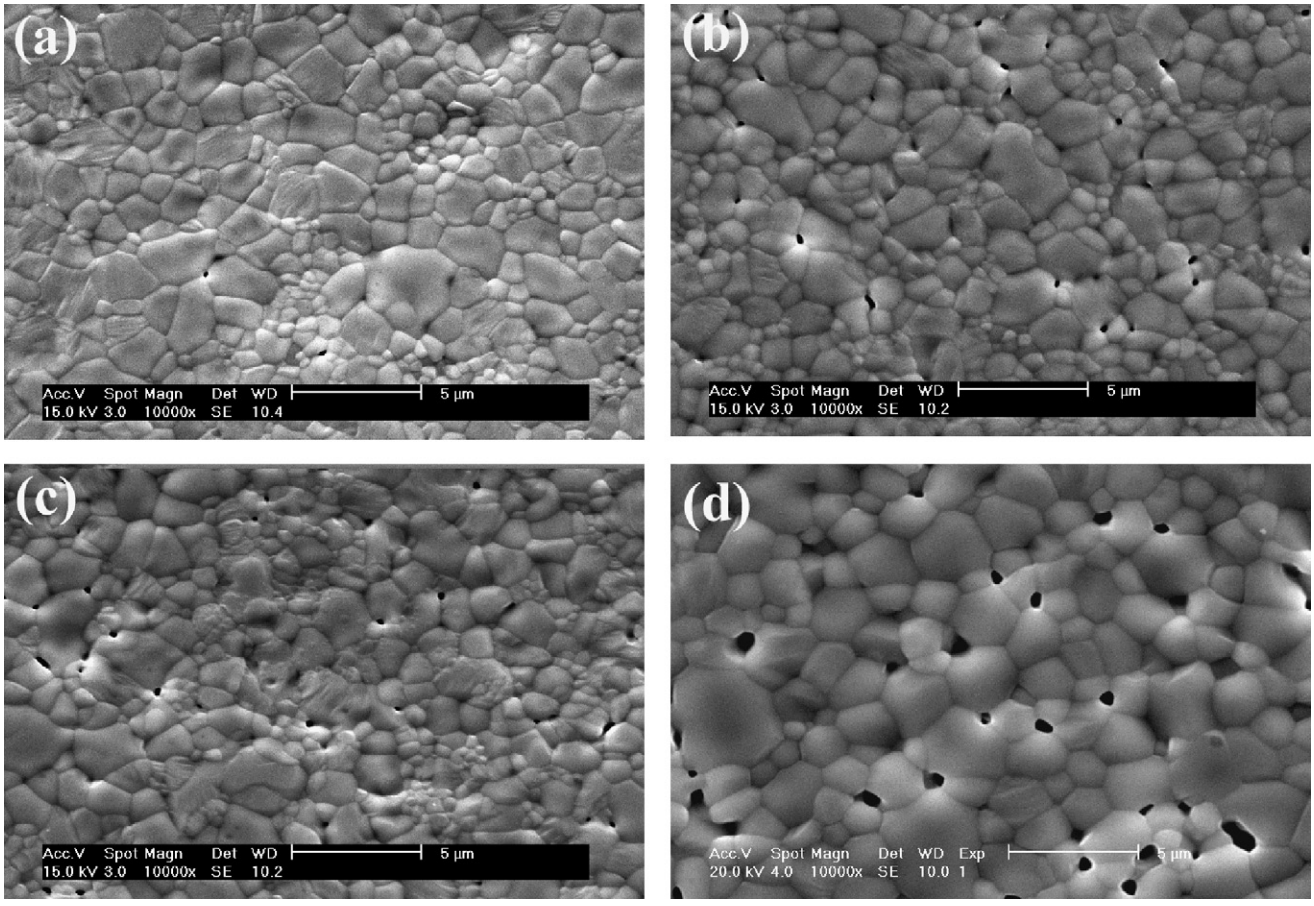

Fig. 3. Scanning electron micrographs of hot pressed pellets of $La_{9.33}(SiO_4)_6O_2$ with porosity = 12% (a), 22% (b), 30% (c) and 33% (d).

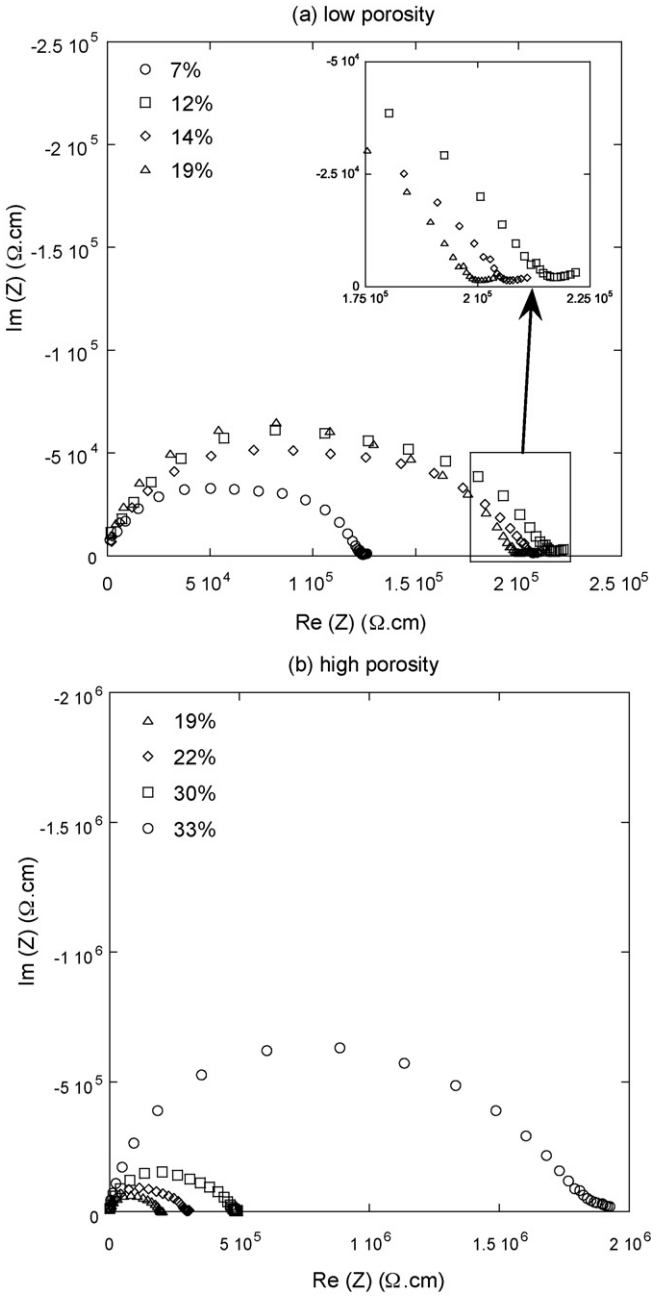

Fig. 4. Impedance plots of hot pressed samples of $La_{9,33}(SiO_4)_6O_2$ in Nyquist format (low porosity samples (a) and high porosity samples (b)).

(=8.8542 pF cm^{-1}), respectively. The evolutions of the real and imaginary parts of the modulus with the frequency of all the samples showed a jump of M' and a peak of M'' in the high frequency region, which are significant of the bulk electrical response.

As a consequence, spectra refinements have been performed attributing the high frequency response to the bulk contribution and the mid frequency response to the grain boundaries contribution. Refinements results are given in Table 1. Resistance and capacity of each contribution are reported after normalization with geometrical factor of the pellets in order to make meaningful comparison of the results. Relaxation frequencies of each contribution are also reported.

The grain boundaries resistance is globally not much affected by the evolution of porosity, except for the most porous samples (30 and 33%), whereas the bulk resistance globally increases with porosity (with a drastic increase for the most porous sample). The highly resistive discontinuous behavior of both contributions of the most porous samples may highlight that the percolation threshold of porosity is reached when it is greater than 30%. It is surprising to notice that intergranular porosity mainly affects the bulk contribution as the grain boundaries contribution remains invariant. Further observations of SEM micrographs (Fig. 3) reveal that intergranular porosity is exclusively located at triple points of the microstructure. An assumption can consist in considering the porosity as air inclusions in the sintered material, which can be assimilated to an apatite-air composite material. As a consequence, all electrical properties deduced from refinement of the high frequency circle will be considered as ‘‘apparent’’ properties of the apatite-air composite.

3.3.2. Activation energy

Fig. 5 presents the temperature dependence of bulk conductivity of all the samples in an Arrhenius format:

$$\sigma = \sigma_0 \exp\left(-\frac{\Delta E_a}{kT}\right)$$

where σ, σ_0, ΔE_a, k and T are, respectively, the conductivity, pre-exponential factor, activation energy, Boltzmann constant and absolute temperature. The increase of the deduced activation energies with the porosity is presented in Fig. 6. Activation energy is correlated to a microscopic phenomenon (oxide ions displacement in the apatite structure), whereas porosity lies at a

Table 1
Refined parameters of impedance plots at 500 °C of $La_{9,33}(SiO_4)_6O_2$ pestles with various porosities

Porosity, %P	Bulk contributions			Grain boundaries contributions		
	R (kΩ cm)	CPE (pF cm^{-1})	ω (10^5 rad s^{-1})	R (kΩ cm)	CPE (nF cm^{-1})	ω (10^4 rad s^{-1})
7	61.4	118	16.01	62.9	1.1	13.50
12	140.1	82	9.85	72.4	0.66	8.52
14	107.6	92	10.34	88.8	1.48	7.10
19	141.9	61	5.29	54.1	1.47	5.25
22	222.6	50	7.94	65.1	0.40	5.97
30	316.1	20	6.19	151.4	0.41	5.48
33	1417.8	15	2.00	343.5	0.66	3.13

NB: Impedance data are systematically normalized with geometrical factor of the pellets (thickness/surface).

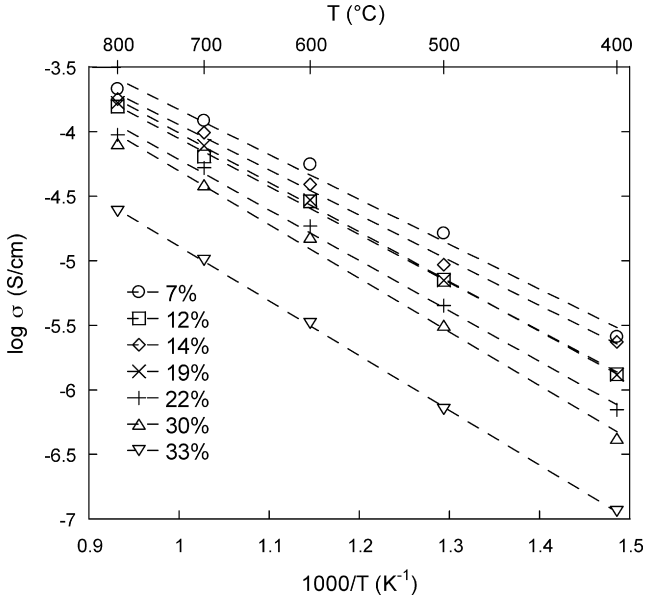

Fig. 5. Temperature dependence of the bulk conductivity of hot pressed sample of $La_{9.33}(SiO_4)_6O_2$.

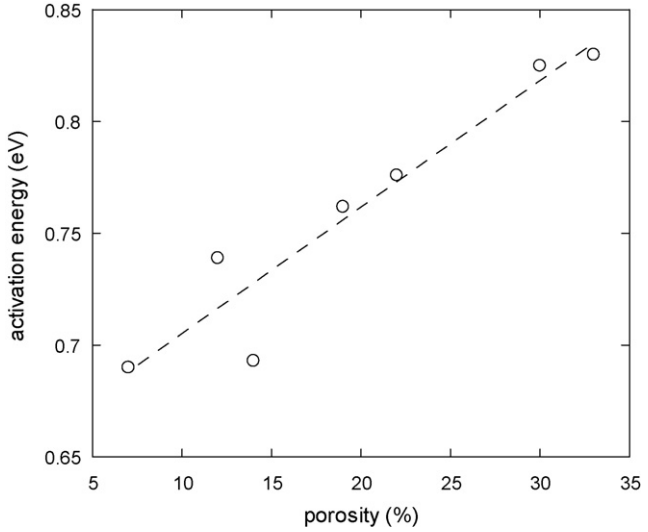

Fig. 6. Porosity dependence of the activation energy of hot pressed sample of $La_{9.33}(SiO_4)_6O_2$.

macroscopic scale: it is not obvious to link these two parameters in a first time. An eventual explanation consists in a modification of the threads of current. In a perfectly densified material, these threads are supposed to be globally parallel to the electric field. The threads of current may have to go round the air inclusions in a porous sample, which may require a higher energy to cross the pellets: the "measured volume" is not the "real volume" of the material.

3.3.3. Conductivity

Previous studies have already shown that the porosity dependence of the ionic conductivity of a ceramic material could be expressed with the Archie's law [31,33,36,38]:

$$\sigma = \sigma_0 \langle \mathrm{vol} \rangle^n$$

where σ is the apparent conductivity of the porous material, σ_0 the intrinsic conductivity of the dense material, $\langle \mathrm{vol} \rangle$ the fraction of material and n a phenomenological parameter. Fig. 7 shows the evolution of the logarithm of σ with the logarithm of the fraction of apatite at several temperatures. Experimental data globally follow the Archie's law with $n = 8.5$, 7.7, 6.9, 6.1 and 5.6 at 400, 500, 600, 700 and 800 °C, respectively, except the conductivity of the most porous pellet (33%), which is much lower than expected. This tends to underline that the percolation threshold of porosity is reached when it is greater than 30%: the behavior of this sample cannot be linked to the same law as less porous pellets.

The constant decrease of n with temperature means that the influence of porosity decreases when the temperature increases. This result is consistent with the higher values of activation energy observed for the most porous samples.

The intrinsic conductivity of a dense pellet (σ_0) can be evaluated after extrapolation to $\langle \mathrm{vol} \rangle = 1$ of Archie's law for each temperature: this can lead to draw a theoretical Arrhenius plot of a non-porous material (Fig. 8). The deduced activation energy is 0.66 eV. This result can be compared to the porosity dependence of activation energy in Fig. 6. If this evolution is linear, an extrapolation to porosity = 0% gives an activation energy of 0.65 eV for a non-porous material. The correlation between these two results first suggests that the porosity

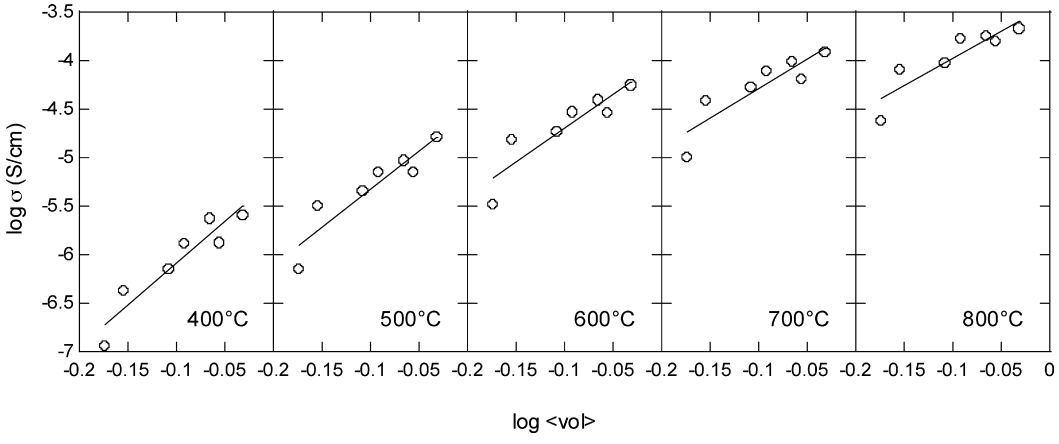

Fig. 7. Evolution of conductivity with the apatite proportion of hot pressed sample of $La_{9.33}(SiO_4)_6O_2$ at several temperatures.

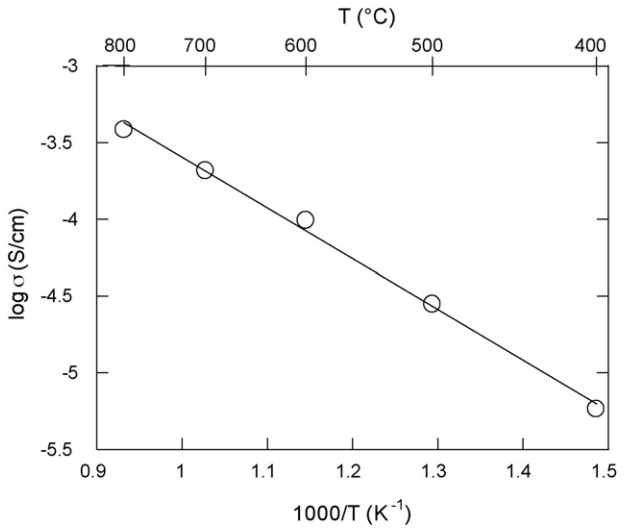

Fig. 8. Calculated temperature dependence of a perfectly densified pellet of $La_{9.33}(SiO_4)_6O_2$.

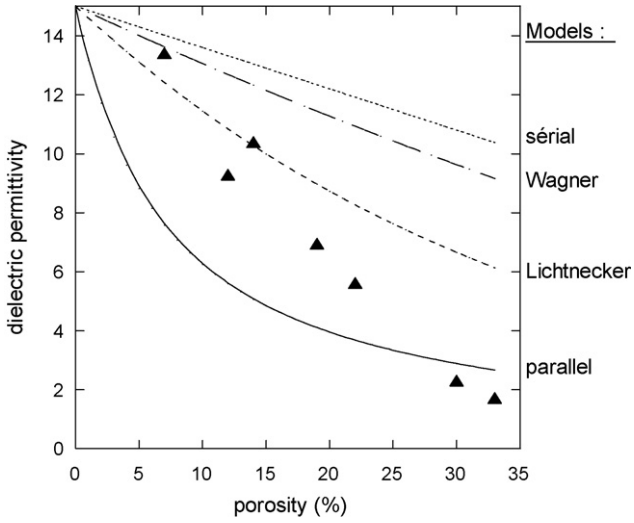

Fig. 10. Porosity dependence of dielectric permittivity of hot pressed pellets of $La_{9.33}(SiO_4)_6O_2$ at 500 °C with several theoretical association models.

dependence of activation energy is quite linear in the range from 0 to 33%. Furthermore, Archie's law seems to be a well-adapted model to describe the porosity dependence of conductivity below the percolation threshold of porosity.

3.3.4. Permittivity

Dielectric permittivity can be deduced from the refined values of capacity associated to the bulk response:

$$C = \varepsilon\varepsilon_0 \frac{S}{t}$$

where C is the capacity associated to the relaxation frequency of the bulk response, ε the dielectric permittivity of the material, ε_0 the vacuum permittivity (8.8542 pF cm^{-1}), S the surface of the pellet and t its thickness. The porosity dependence of dielectric permittivity is presented in Fig. 9 for several temperatures. Dielectric permittivity tends to decrease regularly with increasing porosity. Dipolar relaxation is affected by the presence of porosity in the material: as a consequence it can be supposed that the measured permittivity ε is the apparent permittivity ε_{app} of the apatite-air composite. The influence of porosity does not seem to be affected by the temperature, unlike in other ionic conductors as YSZ [30] and BIMEVOX [33].

The apparent dielectric permittivity of the apatite-air composite can also be estimated by considering several laws of electrical associations. The dielectric permittivity of dense oxyapatite can be approximated to $\varepsilon_s = 15$ after linear extrapolation to porosity = 0% of the graphs in Fig. 9. The dielectric permittivity of air inclusions is $\varepsilon_i = 1$.

Serial and parallel associations are the two extremes models: $\varepsilon_{app,//} < \varepsilon_{app} < \varepsilon_{serial}$. They can be expressed as follow [39]:

$$\varepsilon_{app,série} = P + (1-P)\varepsilon_s; \qquad \varepsilon_{app,//} = \frac{\varepsilon_s}{P(\varepsilon_s - 1) + 1}$$

where P is the fraction of porosity in the material ($0 < P < 1$).

The apparent permittivity of a biphasic material can be expressed by Wagner's law, which considers that a continuous phase (apatite) surrounds isolated inclusions (air = porosity) [39]:

$$\varepsilon_{app} = \varepsilon_s \frac{\varepsilon_i - (1-D)(1-P)(\varepsilon_i - \varepsilon_s)}{\varepsilon_s + D(1-P)(\varepsilon_i - \varepsilon_s)}$$

where D is a depolarization factor. It is equal to 1/3 for spherical inclusions.

Lastly, it can be assumed that there are as many parallel associations as serial associations in the material, which leads

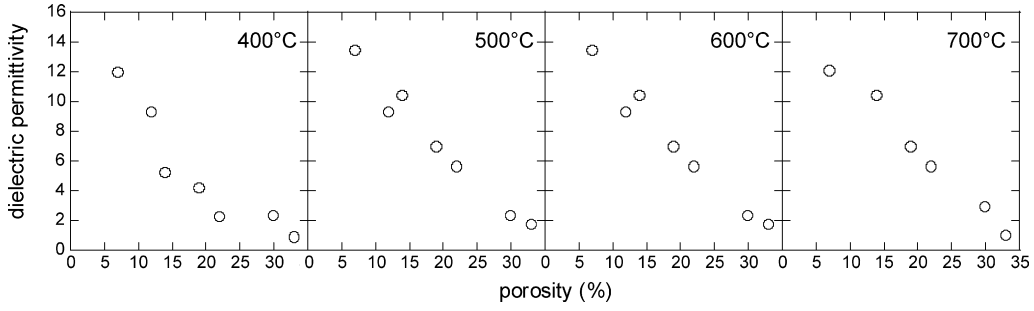

Fig. 9. Porosity dependence of dielectric permittivity of hot pressed pellets of $La_{9.33}(SiO_4)_6O_2$ at several temperatures.

to Lichtenecker's law [39]:

$$\log(\varepsilon_{app}) = (1 - P)\log(\varepsilon_s)$$

The porosity dependence of dielectric permittivity at 500 °C is superposed to the models described above in Fig. 10. These models make assumptions on the material's topology. None of them seems to be perfectly adapted here: experimental points are closer to the serial association model for the lowest porosities and then tend to be closer to the parallel association model. Wagner and Lichtenecker laws might be too simple to render the real topology of the material. The existence of the porosity threshold beyond 30% requires a model that takes this phenomenon into account, as, for instance, the effective medium theory.

4. Conclusion

Oxide ion conductor $La_{9.33}(SiO_4)_6O_2$ has been prepared by solid state reaction synthesis at high temperature. Homogeneous grain size repartition has been obtained by attrition grinding of the powder. Densification by hot pressing gave several pellets with very close microstructural properties and various porosities rising from 7 to 33%.

The influence of the porosity on the electrical properties of the sintered samples has been investigated by impedance measurements. Surprisingly, the high frequency response (attributed to the bulk contribution) was more affected than the mid frequency response (attributed to the grain boundaries contribution) by the intergranular porosity. The exclusive location of the porosity at the triple points of the microstructure led us to consider the sintered pellets as composite materials in assimilating the porosity to air inclusions in the apatite matrix.

The porosity dependence of electrical properties such as conductivity and dielectric permittivity has been explained by using classical composite materials association laws. A constant increase of activation energy with increasing porosity has also been reported, revealing a potential modification of the threads of current in the porous material. The existence of a percolation threshold for porosity values greater than 30% has been underlined, involving great limitation of the electrical performances of the material.

Further studies on the microstructural dependence of the electrical properties of the sintered samples should be practiced. The existence of a mid frequency contribution attributed to the grain boundaries contribution is another parameter increasing the global electrical resistance of the densified material: elaboration of samples with various grain size could bring further information on the influence of grain boundaries on the ionic conductivity process in polycrystalline oxyapatite.

References

[1] O. Yamamoto, Solid oxide fuel cell: fundamental aspects and prospects, Electrochim. Acta 45 (2000) 2423–2435.

[2] N.Q. Minh, T. Takahashi, Science and Technology of Ceramic Fuel Cells, Elsevier, 1995.

[3] N.Q. Minh, Ceramic fuel cells, J. Am. Ceram. Soc. 76 (3) (1993) 563–588.

[4] X.J. Chen, K.A. Khor, et al., Influence of microstructure on the ionic conductivity of yttria-stabilized zirconia electrolyte, Mater. Sci. Eng. A 335 (2002) 246–252.

[5] J.C. Elliott, Structure and Chemistry of the Apatites and Other Calcium Orthophosphates, Elsevier, Amsterdam, 1994.

[6] E.J. Abram, D.C. Sinclair, et al., A novel enhancement of ionic conductivity in the cation-deficient apatite $La_{9.33}(SiO_4)_6O_2$, J. Mater. Chem. 11 (2001) 1978–1979.

[7] J.E.H. Sansom, D. Riching, et al., A powder neutron diffraction study of the oxide-ion-conducting apatite-type phase, $La_{9.33}Si_6O_{26}$ and $La_8Sr_2Si_6O_{26}$, Solid State Ionics 139 (2001) 205–210.

[8] M. Takahashi, K. Uematsu, et al., Single-crystal growth and structure determination of a new oxide apatite, $NaLa_9(GeO_4)_6O_2$, J. Solid State Chem. 139 (1998) 304–309.

[9] S. Nakayama, M. Sakamoto, et al., Oxide ionic conductivity of apatite type $Nd_{9.33}(SiO_4)_6O_2$ single crystal, J. Eur. Ceram. Soc. 19 (1999) 507–510.

[10] H. Benmoussa, M. Mikou, et al., Electrical properties of lanthanum containing vanadocalcic oxyapatite, Mater. Res. Bull. 35 (2000) 369–375.

[11] H. Benmoussa, M. Mikou, et al., Synthesis an physicochemical study of new rare-earth-containing vanadocalcic oxyapatites, Mater. Res. Bull. 34 (9) (1999) 1429–1434.

[12] P. Berastegui, S. Hull, et al., A structural investigation of $La_2(GeO_4)O$ and alkaline-earth-doped $La_{9.33}(GeO_4)_6O_2$, J. Solid State Chem. 168 (2002) 294–305.

[13] A. Bouhaouss, A. Laghzizil, et al., Mechanism of ionic conduction in oxy and hydroxyapatite structure, Int. J. Inorg. Mater. 3 (2001) 743–747.

[14] J. Carpéna, L. Boyer, et al., Ca^{2+}, $PO_4^{3-} = Ln^{3+}$, SiO_4^{4-} coupled substitution in the apatite structure: stability of the mono-silicated fluorbritholite, Earth Planetary Sci. 333 (2001) 373–379.

[15] J.A. Fahey, A. Weber, The Crystal Structure and Stoichiometry of the $Ca_{2+x}Nd_{8-x}(SiO_4)_6O_{2-0.5x}$ System, The Rare Earths in Modern Science and Technology, vol. 3, Plenum Publishing Corporation, 1982 pp. 341–344.

[16] J.A. Fahey, W.J. Weber, et al., An X-Ray and neutron powder diffraction study of the $Ca_{2+x}Nd_{8-x}(SiO_4)_6O_{2-0.5x}$ system, J. Solid State Chem. 60 (1985) 145–158.

[17] A. Serret, M.V. Cabanas, et al., Stabilization of calcium oxyapatites with lanthanum(III)-created anionic vacancies, Chem. Mater. 12 (2000) 3836–3841.

[18] S. Nakayama, H. Aono, et al., Ionic conductivity of $Ln_{10}(SiO_4)_6O_3$ (Ln = La, Nd, Sm, Gd and Dy), Chem. Lett. (1995) 431–432.

[19] S. Nakayama, M. Higuchi, Electrical properties of apatite-type oxide ionic conductors $RE_{9.33}(SiO_4)_6O_2$ (RE = Pr, Nd and Sm) single crystals, J. Mater. Sci. Lett. 20 (2001) 913–915.

[20] S. Nakayama, M. Sakamoto, Electrical properties of new type high oxide ionic conductor $RE_{10}Si_6O_{27}$ (RE = La, Pr, Nd, Sm, Gd, Dy), J. Eur. Ceram. Soc. 18 (1998) 1413–1418.

[21] M. Higuchi, K. Kodaira, et al., Nonstoichiometry in apatite-type neodymium silicate single crystals, J. Cryst. Growth 261 (2000) 317–321.

[22] S. Nakayama, M. Sakamoto, Ionic conductivities of apatites-type $La_x(GeO_4)_6O_{1.5x-12}$ (x = 8–9.33) polycrystals, J. Mater. Sci. Lett. 20 (2001) 1627–1629.

[23] P.J. Panteix, I. Julien, et al., Synthesis and characterization of oxide ion conductors with the apatite structure for intermediate temperature SOFC, Mater. Chem. Phys. 95 (2005) 313–320.

[24] S.P.S. Badwal, F.T. Ciacchi, et al., An investigation of conductivity, microstructure and stability of electrolyte compositions in the system 9 mol% (Sc_2O_3–Y_2O_3)–$ZrO_2(Al_2O_3)$, Solid State Ionics 109 (1998) 167–186.

[25] I.R. Gibson, G.P. Dransfield, et al., Sinterability of commercial 8 mol% yttria-stabilized zirconia powders and the effect of sintered density on the ionic conductivity, J. Mater. Sci. 33 (1998) 4297–4305.

[26] D.Z. de Florio, R. Muccillo, Sintering of zirconia-yttria-ceramics studied by impedance spectroscopy, Solid State Ionics 123 (1999) 301–305.

[27] J. Van herle, R.V. Cavieres, et al., Microstructure-conductivity correlation for hot-pressed 8YSZ powders, J. Eur. Ceram. Soc. 21 (2001) 1851–1854.

[28] M.J. Jorgensen, S. Primdahl, et al., Effect of sintering temperature on microstructure and performance of LSM–YSZ composite cathodes, Solid State Ionics 139 (2001) 1–11.

[29] B. Kumar, C. Chen, et al., Electrical properties of heterogeneously doped yttria-stabilized zirconia, J. Power Sources 140 (2005) 12–20.
[30] M. Kleitz, L. Dessemond, et al., Model for ion-blocking at internal interfaces in zirconias, Solid State Ionics 75 (1995) 107–115.
[31] M. Kleitz, M.C. Steil, Microstructure blocking effect versus effective medium theories in YSZ, J. Eur. Ceram. Soc. 17 (1997) 819–829.
[32] M. Benkaddour, M.C. Steil, et al., The influence of particle size on sintering and conductivity of $Bi_{0,85}Pr_{0,105}V_{0,045}O_{1,545}$ ceramics, J. Solid State Chem. 155 (2000) 273–279.
[33] M. Benkaddour, P. Conflant, et al., Evolution of microstructure and impedance upon the sintering of a Bi–Pr–V-based fluorite type oxide conductor, Solid State Ionics 146 (2002) 175–184.
[34] B.C.H. Steele, Appraisal of $Ce_{1-y}Gd_yO_{2-y/2}$ electrolytes for IT-SOFC operation at 500 °C, Solid State Ionics 129 (2000) 95–110.
[35] C. Tian, S.W. Chan, Ionic conductivities, sintering temperatures and microstructures of bulk ceramic CeO_2 doped with Y_2O_3, Solid State Ionics 134 (2000) 89–102.
[36] S. Georges, Etude de nouveaux conducteurs par ions O^{2-} dérivés de $La_2Mo_2O_9$, Université du Maine, Le Mans, 2003.
[37] S. Georges, Zlive program, http://www.univ-lemans.fr/sciences/fluorures/ldf.html.
[38] G.E. Archie, The electrical resistivity log as an aid to determining some reservoir characteristics, Trans. AIME 146 (1942) 54–62.
[39] P. Abélard, P. Boch, et al., Propriétés et applications des céramiques, Hermes Science Publications, 2001.